Metal-Dielectric Coaxial Dual-Mode Resonator Bandpass Filters

Yuliang Chen, *Graduate Student Member, IEEE*, and Ke-Li Wu, *Fellow, IEEE*

***Abstract*— A metal-dielectric coaxial (MDC) dual-mode resonator for bandpass filters is proposed in this work and is applied to various practical filter realizations in a compact in-line layout. Since the MDC resonator supports the TEM mode of the metal coaxial resonator and one of HE_{11} modes of a metal-loaded dielectric resonator (DR), both of which are dissimilar fundamental modes, the dual-mode resonator occupies a comparable volume that a conventional coaxial resonator can achieve. In addition to the basic properties of the dual-mode resonator, the mechanisms for controlling the couplings between various modes are also discussed in detail. The in-line realization of the cascaded quadruplet (CQ) and cascaded triplet (CT) sections using the MDC dual-mode resonator are particularly investigated for facilitating the design of practical filters with different filtering characteristics. To demonstrate the applicability of the proposed MDC dual-mode resonator, three six-pole bandpass filter prototypes in the in-line configuration are designed, fabricated, and tuned in the 3.5-GHz band with different transmission zero (TZ) arrangements. All experimental results affirm the unique features of the MDC dual-mode resonator and demonstrate its applicability to compact in-line bandpass filters with a wide range of symmetric/asymmetric filtering responses for future wireless base stations.**

***Index Terms*— Dual-mode resonator, filter miniaturization technique, in-line layout, transmission zero (TZ).**

I. Introduction

As essential components in radio frequency (RF) front ends of base stations for wireless communication systems with advanced air-interface architecture, such as massive multi-input–multi-output (M-MIMO), bandpass filters increasingly face challenging demands in terms of higher near passband rejection, lower insertion loss, less volume and weight, and more desire for in-line physical layout [1]. Among notable efforts in overall size reduction, adoption of dielectric resonator (DR) and utilization of multimode resonators are always the two most popular options among many others, which provide not only a low loss but also a good thermal stability solution [2], [3]. The early works on DR filters were well reviewed in [4]. In most existing DR filter structures, the dielectric puck is situated in a metal housing cavity. Thus, the resonant frequency and the unloaded Q of a particular mode are determined by both the dielectric puck and dimensions of the cavity. Regarding the multimode resonator filters, the dual-mode DRs have demonstrated their viability in practical applications. Some representative configurations of dual-mode DRs include the dielectric-loaded circular waveguide resonator that supports dual degenerate TE_{111} modes [5], the dual-mode DR combined with a conductor loaded dual-mode resonator [6], the cavity resonator loaded by grooved/splitted ceramic disks that is convenient to enhance the couplings [7], the dual TM_{110} (also called HE_{11}) mode resonator for a compact filter array in a planar layout [8], and the dual HE_{11} mode conductor-loaded DR for high unloaded Q [9]. Although the degenerate HE_{11} modes can be managed to be the fundamental modes by increasing the height of housing cavity, due to the nature of the degenerate modes and the increased housing cavity size, the volume saving compared to a dielectric-loaded single-mode resonator is only about 30% [10, p. 526]. Moreover, due to the spatial orthogonality of degenerate modes, it is practically difficult to construct a dual-mode filter in the in-line layout. The crowd of higher order spurious resonances near the passband is always a concern in utilizing such a dual-mode resonator filter.

It is worth mentioning that although the feasibility of triple-mode DR resonators has been studied by employing different types of degenerate modes in a dielectric-loaded housing cavity [11], [12], [13], the flexibility in filter coupling topology is inevitably limited and the independence of controlling required couplings is known to be practically difficult if not impossible.

Except exploiting degenerate modes for dual-mode resonators, utilizing two dissimilar fundamental resonant modes in one physical cavity has shown to be another promising option for maximizing size reduction of a resonator. In this direction, a new type of dielectric-loaded waveguide dual-mode resonator employing TE_{101} mode and a dielectric $TE_{01\delta}$ mode is proposed in [14]. A three-quarter wavelength long coaxial resonator is horizontally situated in a rectangular waveguide resonator, forming another kind of dual-mode waveguide resonator with two dissimilar fundamental modes: the TEM mode and cavity TE_{101} mode [15]. To maximize the size reduction, a dual-mode monoblock DR (MDR) filter utilizing two perpendicular dissimilar TEM modes is reported in [16]. Compared to the conventional degenerate dual-mode

Manuscript received 28 June 2023; revised 10 August 2023; accepted 11 August 2023. This work was supported by the Postgraduate Scholarship from The Chinese University of Hong Kong. This article is an expanded version from the 2023 International Microwave Symposium, San Diego, CA, June 11–16, 2023. *(Corresponding author: Ke-Li Wu.)*

The authors are with the Department of Electronic Engineering, The Chinese University of Hong Kong, Shatin, Hong Kong (e-mail: ylchen@link.cuhk.edu.hk; klwu@cuhk.edu.hk).

Color versions of one or more figures in this article are available at https://doi.org/10.1109/TMTT.2023.3306590.

Digital Object Identifier 10.1109/TMTT.2023.3306590

resonators, the superiorities of such dissimilar fundamental dual-mode resonators are apparent: 1) both dissimilar modes are fundamental modes supported by their own resonant mechanism so that the size reduction can be maximized, and 2) the higher order resonances related to each dissimilar fundamental mode are far away from that of the fundamental modes and can be staggered, and hence, the spurious-free frequency band is comparable to that of a single fundamental mode resonator.

Needless to say, metal coaxial resonator filters, or combline filters, still dominate the application for base station filters even for M-MIMO radio front ends due to their relatively low cost, favorable tradeoff between the size and unloaded Q, and great flexibility in realizing various coupling topologies. However, there is no effective way to reduce the size of a coaxial resonator filter without severely sacrificing the unloaded Qs. Due to the significant increase in the number of channel filters for M-MIMO base stations, tremendous pressure on size reduction is imposed on the industry, to whom the in-line layout is highly desirable to fit a compact filter array containing multiple filters of the same characteristics. Recently, some efforts have been paid to the filters with in-line topology from filter synthesis point of view [17]. However, there is not enough attention putting eyes on new in-line physical realization of high-performance bandpass filters with various transmission zero (TZ) arrangements.

In this work, a new class of metal-dielectric coaxial (MDC) dual fundamental mode resonator filters are presented. The resonator configuration is elicited from the working principles of a metal coaxial resonator and a grounded DR in a metal cavity. The proposed dual-mode resonator supports two dissimilar fundamental modes: the TEM mode of a metal coaxial resonator and a dielectric HE_{11} mode. By appropriately arranging the maximum of the magnetic field lines of the HE_{11} mode, the commonly used coupling sections, such as cascaded triplet (CT) and cascaded quadruplet (CQ), can be realized in a true in-line configuration. In addition to the thorough discussion on the basic working principle of the MDC dual-mode resonator, the coupling structure and the suppression mechanism of the other degenerate HE_{11} mode are presented in great detail in this article. Moreover, the in-line triplet section with an MDC dual-mode resonator is elaborated and demonstrated by two filter prototypes, presenting a significant expansion on the work in [18]. The unique and attractive features of the new dual-mode resonator include: 1) up to 50% volume reduction due to employment of two fundamental modes; 2) high suitability of in-line physical layout; 3) high unloaded Qs for the dual modes; and 4) a wide spurious rejection band.

To validate the new dual-mode resonator and to demonstrate its applicability to commonly used coupling topologies, three bandpass filters in the 3.5-GHz band are designed, fabricated, and tuned. The prototyped filters include a six-pole in-line bandpass filter with a CQ section and two six-pole in-line bandpass filters with symmetric and asymmetric responses realized by two CT sections. Experimental results verify that the proposed MDC dual-mode resonator is a viable candidate for compact bandpass filters in an in-line configuration.

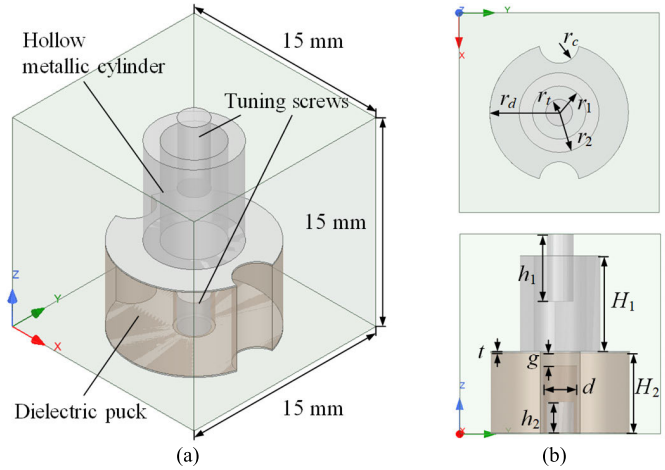

Fig. 1. (a) Isometric view of the proposed MDC dual-mode resonator with outer dimensions. (b) Top view and side view of the MDC dual-mode resonator with dimensional parameters.

II. MDC Dual-Mode Resonator

The basic structure of the proposed MDC dual-mode resonator is shown in Fig. 1(a). For typical 3.5-GHz applications, the outer dimensions of the metal housing are $15 \times 15 \times 15$ mm^3, which is in the same range as that for a conventional single-mode metal coaxial resonator cavity. A grounded cylindrical dielectric with two semicircle grooves is positioned at the center of the cavity with its top surface metalized. A metal hollow cylinder is coaxially mounted on the top of the DR. In the electromagnetic (EM) model of the demonstration example, the dielectric material is with a relative permittivity $\varepsilon_r = 39.5$ and a loss tangent $\tan\delta = 5 \times 10^{-5}$, and the metal conductivity of the silver-plated top and the metallic cavity housing is $\sigma = 2 \times 10^7$ S/m. Provision of two tuning screws is also provided in the EM model.

A. Dual-Mode Resonator

To understand the basic properties of the two resonant modes, an HFSS EM model is built with critical dimensions labeled in Fig. 1(b), which are set initially as $r_1 = 2$ mm, $r_2 = 3$ mm, $r_d = 5.2$ mm, $H_1 = 7.15$ mm, $H_2 = 6$ mm, $d = 2.5$ mm, and $g = 1$ mm. The radius of both tuning screws is $r_t = 1$ mm, and their depths are marked as h_1 and h_2.

Having conducted eigenmode analysis for resonant mode patterns and frequencies, the TEM mode (called mode 1) is always preserved. When the depth of the tuning screw $h_1 = 4$ mm, the resonant frequency of mode 1 is $f_1 = 3.6$ GHz, and its unloaded Q is 1900.

By choosing appropriate dimensions, the resonant frequency of an HE_{11} mode, called HE_{11a} mode, can be observed near that of the TEM mode. To create a dual dissimilar fundamental mode resonator, the other degenerate HE_{11} mode, namely, HE_{11b} mode, is pushed upward by cutting two semicircle grooves, whose radius is r_c, vertically on two sides of the dielectric puck. With $r_c = 1.5$ mm and $h_2 = 2.5$ mm, a parametric study by varying the radius of dielectric puck r_d is presented in Fig. 2(a). It can be seen that the resonant frequencies of both HE_{11} modes and the first higher order

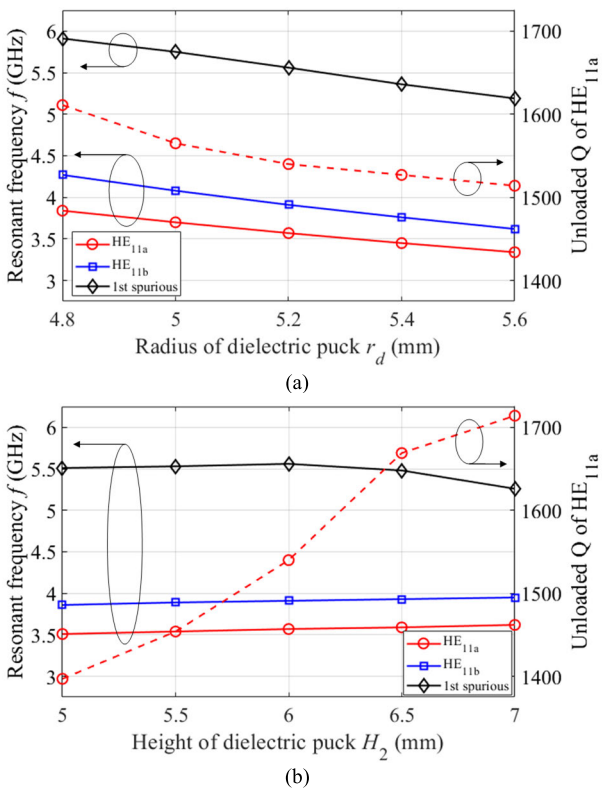

Fig. 2. Resonant frequencies of HE_{11} modes and the first higher order spurious mode, together with the unloaded Q of HE_{11a} mode versus (a) radius r_d for $H_2 = 6$ mm, $r_c = 1.5$ mm, and $h_2 = 2.5$ mm and (b) height H_2 for $r_d = 5.2$ mm, $r_c = 1.5$ mm, and $h_2 = 2.5$ mm.

spurious mode decrease as radius r_d increases, while the unloaded Q of the retained HE_{11a} mode (mode 2) declines very slightly. When $r_d = 5.2$ mm and $H_2 = 6$ mm, the resonant frequency of mode 2 is $f_2 = 3.6$ GHz with an unloaded $Q = 1550$, whereas the frequency of HE_{11b} mode is pushed to 3.91 GHz. The separation of the resonant frequencies of HE_{11a} mode and HE_{11b} mode is sufficiently larger than the bandwidth of the filter to be designed.

Fig. 2(b) shows the parametric study of mode 2 by varying the height of the dielectric puck, showing that the resonant frequencies of both HE_{11} modes and the first higher order spurious mode almost remain unchanged, while the unloaded Q increases as height H_2 increases. Therefore, it can be concluded that the radius r_d can be appropriately adjusted to control the resonant frequency of the HE_{11} mode (mode 2) f_2, whereas its height H_2 dominates the unloaded Q of mode 2.

Fig. 3 shows the magnetic field patterns of the two fundamental modes observed from an *xoy* plane at different heights z. It can be observed that the magnetic field distribution of mode 1 is very similar to that of an ordinary metal coaxial resonator, justifying that the displacement current of the mode in the dielectric puck maintains the continuity of the current on the metal cylinder. Different from mode 1, the magnetic field of mode 2 is only confined in the region near the dielectric puck. The strategies of using the field patterns and further suppressing the unwanted HE_{11b} mode will be discussed in later sessions.

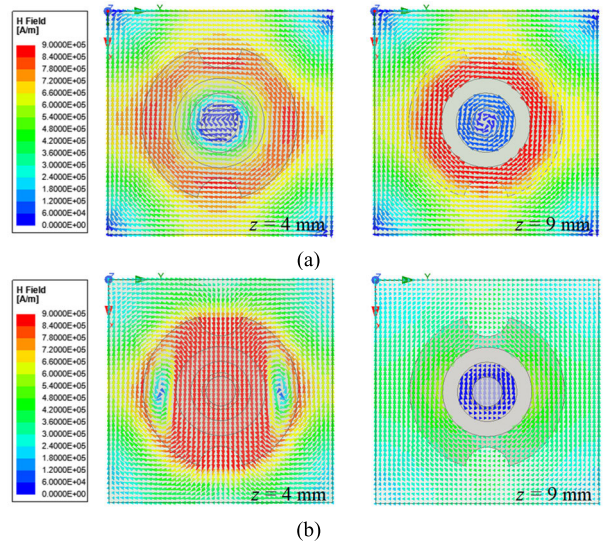

Fig. 3. Magnetic field patterns of the two fundamental modes in the *xoy* plane at different heights z at 3.6 GHz. (a) TEM mode (mode 1) at $z = 4$ mm and $z = 9$ mm. (b) HE_{11a} mode (mode 2) at $z = 4$ mm and $z = 9$ mm.

B. Height Reduction of the Dual-Mode Resonator

Adding a "mushroom" shaped capacitive disk on the top of inner conductor is an effective way to reduce the total height of metal coaxial resonator and has been widely adopted in the wireless industry. For the proposed MDC dual-mode resonator, since the field distribution of the TEM mode is preserved for mode 1, the "mushroom" structure can also be applied to reduce the height of the resonator.

As shown in Fig. 4, with all dimensions of the dielectric puck unchanged, the metal hollow cylinder of the MDC dual-mode resonator in Fig. 4(a) is shortened by 2 mm as shown in Fig. 4(b) by loading the metal resonator with a metal disk of radius of 4.5 mm and a thickness of 0.5 mm. The eigenmode analysis also shows that the unloaded Q of mode 1 slightly reduces by only 4% due to the height reduction but is still 7% higher than that of a conventional single TEM mode resonator with a total height of 15 mm. This is because the low-loss dielectric puck that works as part of the inner conductor post for the TEM mode dominates the loss of the mode.

C. Coupling Between the Dual Dissimilar Modes

Due to the symmetry of the resonator structure from the top view, the coupling between the magnetic field of mode 1 and the two halves of that of mode 2 exactly counteracts. Therefore, it can be intuitively understood that no coupling exists between the two modes in the original MDC dual-mode resonator. However, in constructing a coupled-resonator filter, the perturbation of the modes by the coupling window may inevitably cause a certain amount of coupling between the two modes. Fig. 5 shows the sketch of the magnetic fields of the two modes with different arrangements of the dielectric puck. Both resonators are perturbed by a coupling window. The red and black solid line contours represent the metal cylinder and dielectric puck, respectively. For arrangement 1 shown in

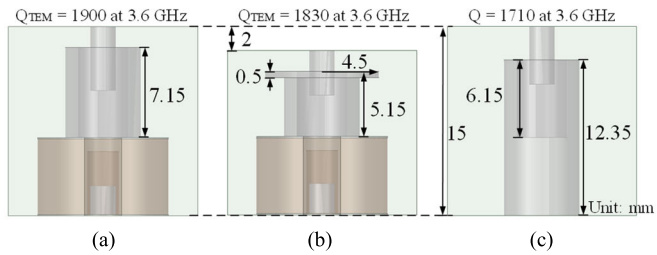

Fig. 4. Structure of different types of resonators (side view) with key dimensional parameters and unloaded Q of TEM mode at 3.6 GHz. (a) Proposed MDC dual-mode resonator. (b) Proposed MDC dual-mode resonator with a "mushroom" structure for height reduction. (c) Conventional single TEM mode resonator.

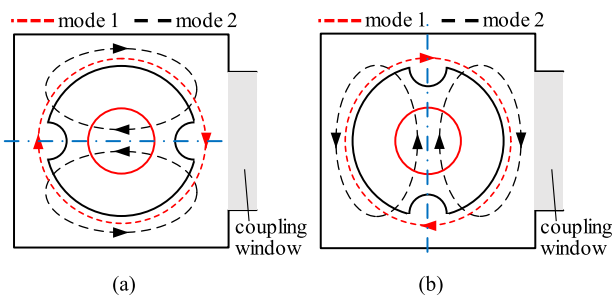

Fig. 5. Magnetic field lines (top view) of the MDC dual-mode resonator with different arrangements of the dielectric puck. (a) Semicircular groove faces the coupling window. (b) Rotate the dielectric puck in arrangement (a) by 90°. Red short dashed lines: magnetic field of the TEM mode (mode 1). Black long dashed lines: magnetic field of the HE_{11a} mode (mode 2). Blue dot-dashed lines: original symmetry axis of H-field distribution in the dual-mode resonator.

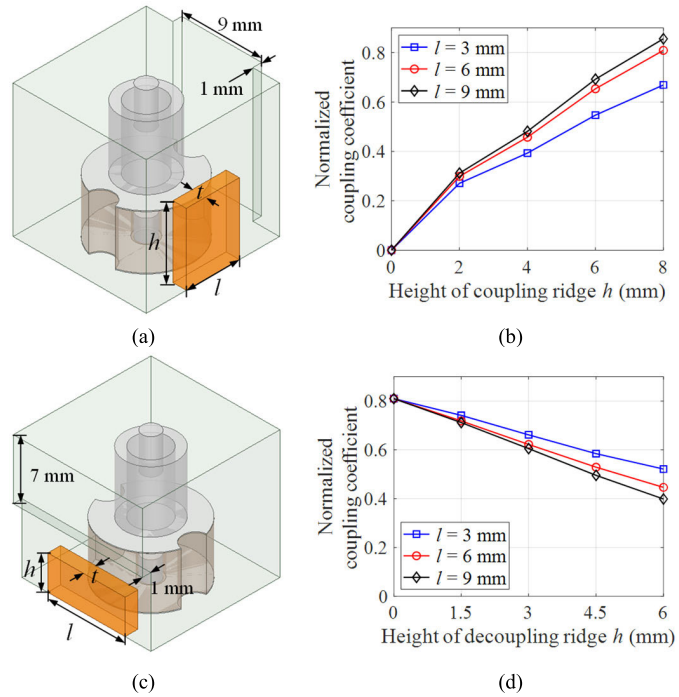

Fig. 6. (a) Isometric view of MDC dual-mode resonator with a partial width coupling window and a coupling ridge. (b) Normalized coupling coefficient between two fundamental modes versus height of coupling ridge h with fixed $t = 1.5$ mm and a different length l. (c) Isometric view of the dual-mode resonator with a partial height coupling window and a decoupling ridge. (d) Normalized coupling coefficient between two fundamental modes versus height h with fixed $t = 1.5$ mm and different lengths l.

Fig. 5(a), the original symmetry of the two fundamental modes is not affected as the two semicircular grooves are on the symmetry axis; thus, the coupling between the two modes is zero. In contrast, for arrangement 2 as shown in Fig. 5(b), the symmetry is spoiled, and thus, the coupling between modes 1 and 2 occurs and needs to be controlled.

The coupling control mechanisms for both arrangements in Fig. 5 are presented and quantitatively analyzed. For arrangement 1, the magnetic field line exhibits a null field at the coupling window, it is an appropriate choice if two TEM modes of two adjacent resonators are coupled with a partial width coupling window. As far as the coupling between the two dissimilar modes in the dual-mode resonator is concerned, as shown in Fig. 6(a), a rectangular metal coupling ridge with height h, length l, and thickness t can be placed at the center of a side wall adjacent to the partial width coupling window to perturb the symmetry of the magnetic fields and control coupling between the two fundamental modes. As shown in Fig. 6(b), for a given length l of the ridge, the coupling coefficient increases as the height h increases. The coupling coefficient of the two modes is calculated by the extraction method introduced in [19] with a center frequency of 3.6 GHz and a bandwidth of 200 MHz.

For arrangement 2, the magnetic field lines of both the TEM and the HE_{11a} modes reach maximum at the coupling window. To couple the TEM modes of two adjacent resonators, a partial height coupling window is appropriate to minimize the unwanted coupling to the HE_{11a} mode. Since the coupling between the two fundamental modes in the dual-mode resonator exists and is likely higher than the required, the decoupling mechanism as shown in Fig. 6(c) is suggested, in which a metal ridge on the wall of the partial height coupling window is introduced. The parametric analysis depicted in Fig. 6(d) shows that the coupling between the two modes becomes smaller as the height h and length l of the decoupling ridge increase.

It is worth noting that for both arrangements, the perturbation effect of the coupling/decoupling ridge can be opposite when the ridge is placed on the opposite side. In practice, one or two tuning screws can be previsioned for the postfabrication tuning process. The tuning screws may be placed near the ridge from the bottom of the dual-mode cavity to compensate the coupling/decoupling ridge.

III. Realizable Coupling Configurations

In this section, the coupling mechanism between two MDC dual-mode resonators as well as in-line coupling structure between a single TEM mode resonator and an MDC dual-mode resonator are elaborated. By appropriately cascading the dual-mode resonator and a single TEM mode resonator, different coupling sections, such as CQ and CT sections, can be constructed, thus facilitating the realization of various filtering characteristics in an in-line configuration.

A. Further Suppression of HE_{11b} Mode

Although the first spurious resonance, HE_{11b} mode, has been pushed out of the passband, to achieve a good spurious

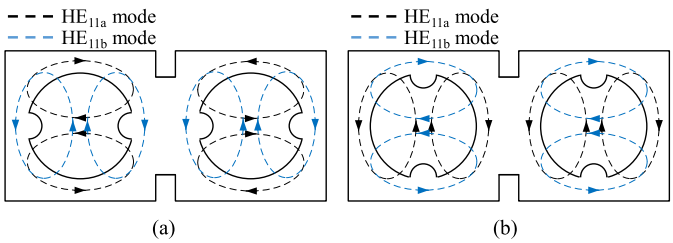

Fig. 7. Magnetic field lines (top view) of two dielectric HE_{11} modes in different coupling configurations for two cascaded MDC dual-mode resonators. (a) Semicircular grooves of both dielectric pucks face the coupling window. (b) Both dielectric pucks in arrangement (a) are rotated by 90°. Black dashed lines: magnetic field of HE_{11a} mode. Blue dashed lines: magnetic field of HE_{11b} mode.

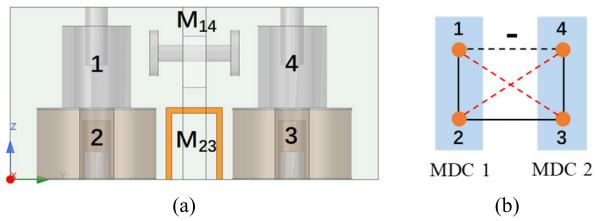

Fig. 8. Coupling configuration for CQ section with two MDC dual-mode resonators. (a) Physical structure (side view). (b) Coupling diagram.

performance in practical applications, the suppression of HE_{11b} mode near the passband must be investigated.

The magnetic fields of the dielectric HE_{11} modes in two cascaded MDC dual-mode resonators are sketched in Fig. 7. For the coupling configuration shown in Fig. 7(a), the semicircular grooves of both dielectric pucks face the inductive coupling window, and thus, the magnetic field of two HE_{11b} modes can be easily coupled, whereas the coupling between two HE_{11a} modes of two dielectric pucks is too weak. The contrary is the case shown in Fig. 7(b). Therefore, the two MDC dual-mode resonators should be cascaded in the way shown in Fig. 7(b) [corresponding to the arrangement of Fig. 5(b)] to suppress the propagation of HE_{11b} mode to the greatest extent. Meanwhile, the coupling between two HE_{11a} modes of two cascaded MDC dual-mode resonators can be easily realized and controlled. By further suppressing its propagation, the unwanted HE_{11b} mode can no longer be a threat as a spurious mode, leading to a relatively wider spurious-free frequency band.

B. Couplings for CQ Section

Fig. 8(a) shows a possible coupling configuration for realizing a CQ section consisting of two MDC dual-mode resonators. In the physical realization, the coupling M_{23} is realized by a partial width window and a grounded loop between dielectric pucks 2 and 3, thus the magnetic fields of two HE_{11a} modes can be coupled. Furthermore, the capacitive cross-coupling M_{14} is realized by a dumbbell-shaped probe between two metal coaxial resonators 1 and 4. Therefore, with the inductive mainline coupling M_{23} and capacitive cross-coupling M_{14}, two TZs, one on each side of the passband, can be created.

The actual coupling diagram of the quadruplet section is shown in Fig. 8(b). A certain amount of parasitic coupling

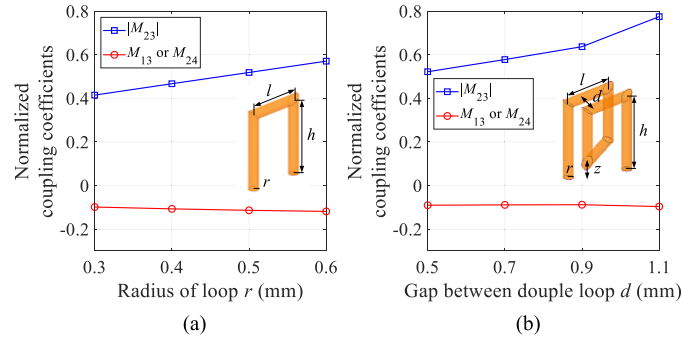

Fig. 9. Parametric study of different grounded loops for CQ section. (a) Single loop for mainline/diagonal coupling versus radius r for $h = 6$ mm and $l = 4.2$ mm. (b) Double loop for mainline/diagonal coupling versus gap d for $h = 6$ mm, $l = 4.2$ mm, $r = 0.3$ mm, and $z = 1.5$ mm.

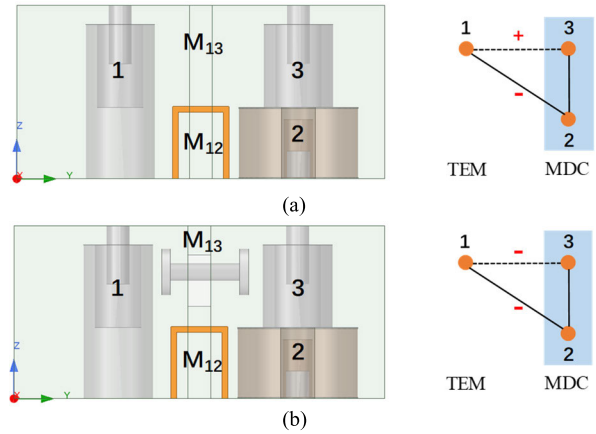

Fig. 10. Coupling configurations for CT section formed by a single TEM mode and an MDC dual-mode resonator. Physical structure (side view) for one TZ at (a) lower side and its coupling diagram and (b) higher side and its coupling diagram.

(M_{13} and M_{24}) arises between the TEM mode (mode 1) in one cavity and the HE_{11a} mode (mode 2) in another cavity since the magnetic field of mode 1 exists along the height of the dual-mode cavity. Due to the symmetry of the structure, the two diagonal parasitic couplings can be assumed to be equal. In order to reduce the parasitic coupling and enhance the mainline coupling M_{23}, a double loop structure with a detailed parametric study has been discussed in [18] and is also presented in Fig. 9, for which the center frequency and the bandwidth are set as 3.6 GHz and 125 MHz, respectively.

C. Couplings for CT Section

Although the aforementioned CQ section can produce a pure imaginary TZ pair with one on each side of the passband, the relative positions of the two TZs are affected by the parasitic diagonal coupling. Moreover, the realized fractional bandwidth is limited due to the insufficient coupling between the two dielectric HE_{11a} modes, which is known to be naturally weak for EM fields being trapped inside the dielectrics.

Another commonly used coupling scheme is the triplet coupling section that can be realized by coupling one proposed MDC dual-mode resonator with a metal coaxial single TEM mode resonator, as shown in Fig. 10. The coupling M_{12}

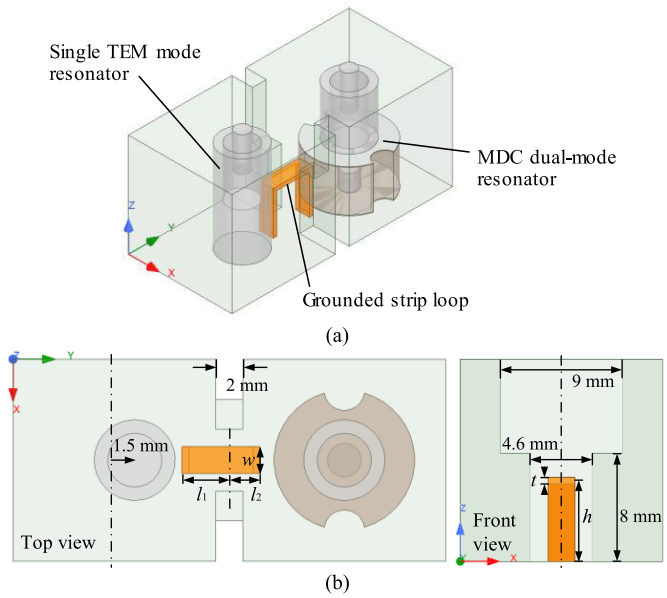

Fig. 11. Coupling structure of the CT section in Fig. 10(a). (a) Isometric view. (b) Top view (with all tuning crews and metallized surfaces removed) and front view (with both resonators removed) with necessary dimensional parameters.

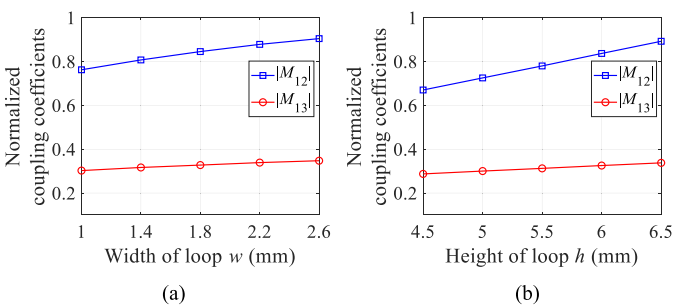

Fig. 12. Parametric study of grounded strip loop for CT section. Absolute value of mainline/cross-coupling versus (a) width w for $h = 6$ mm and (b) height h for $w = 1.7$ mm. Other dimensional parameters are fixed with $t = 0.5$, $l_1 = 3.5$, and $l_2 = 2.25$ (all in mm).

between the TEM mode and the dielectric HE_{11a} mode is realized by a partial width inductive window and can be strengthened by a grounded metal strip loop. The coupling can be adjusted by the dimensions of the coupling window and the width and height of the loop. The cross-coupling M_{13} between the two TEM modes can be easily realized by the inductive window that can be controlled by a tuning screw from the top of the window. For the arrangement shown in Fig. 10(a), the polarities of the mainline coupling M_{12} and the cross-coupling M_{13} are opposite. According to the coupling sign correction theory [10, p. 443], one TZ on the lower side of the passband can be realized by the CT section. As shown in Fig. 10(b), to create one TZ at the upper side of the passband, the cross-coupling M_{13} needs to be realized by a capacitive coupling probe.

With all dimensional parameters and variables labeled in Fig. 11, a parametric study of the grounded strip loop is presented in Fig. 12(a) and (b). To enhance the mainline coupling M_{12}, the inner conductor rod of the single TEM mode resonator is horizontally moved by 1.5 mm from

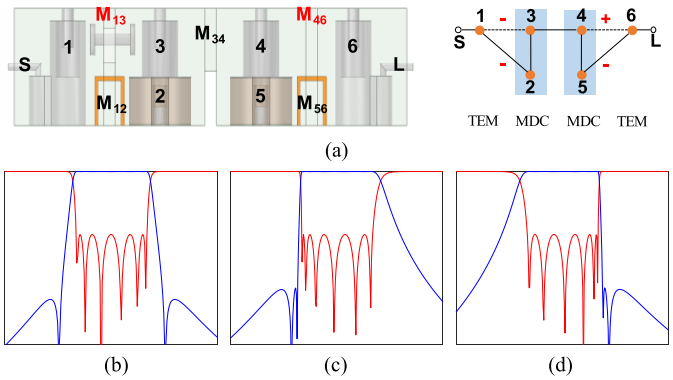

Fig. 13. Sixth-order filter coupling configuration and its possible ideal responses by combining MDC dual-mode resonators with single TEM mode resonators. (a) Physical structure (side view) and coupling diagram of a two-CT in-line layout. (b)–(d) Symmetric/asymmetric responses with other realization of M_{13} and M_{46} of (a).

the cavity center toward the inductive window. The lower part of the inductive window is narrower compared to the upper part to reduce the effect of the grounded loop on the cross-coupling M_{13}. The coupling coefficient is extracted at the center frequency of 3.6 GHz with the bandwidth of 200 MHz. To avoid the sign ambiguity, all the normalized coupling coefficients are marked with their absolute values in Fig. 12. It can be observed that the mainline coupling M_{12} becomes stronger as the width w or the height h of the strip increases, and the cross-coupling M_{13} also increases but at a much slower rate than M_{12}. Therefore, although the inductive window is introduced for both M_{12} and M_{13}, the mainline coupling M_{12} can be independently controlled by adjusting the dimensions of the grounded strip loop. Moreover, it can be found that a sufficiently large M_{12} can be realized in a CT section.

D. Possible In-Line Coupling Configurations

With the proposed MDC dual-mode resonator and the established intercavity coupling sections, some practical filter coupling configurations can then be developed. It is also noteworthy that the conventional CT and CQ sections can be physically laid out in the longitudinal direction using the MDC dual-mode resonator, leading to a true in-line configuration. Moreover, the fractional bandwidth of such filters can be enhanced by introducing the mainline intercavity coupling between the TEM mode in the single-mode resonator and the dielectric HE_{11a} mode, which circumvents the relatively insufficient coupling between two dielectric HE_{11a} modes.

Fig. 13 shows the physical structure, coupling topology, and the typical responses of six-pole 2-TZ (6-2) bandpass filters by combining the MDC dual-mode resonator with two single TEM mode resonators. As shown in the EM model and coupling diagram in Fig. 13(a), two single TEM mode resonators can be combined with two MDC dual-mode resonators to construct two CT sections. Section 1-2-3 consists of a capacitive coupling probe for negative cross-coupling M_{13} and produces a TZ at the upper side of the passband, and section 4-5-6 is with a partial width coupling window for

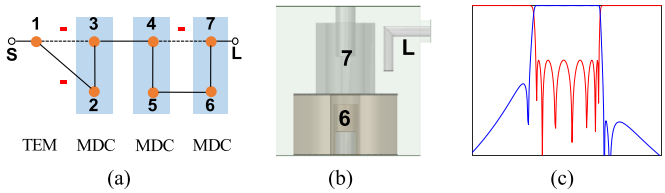

Fig. 14. Seventh-order filter with three TZs using MDC dual-mode and single TEM mode resonators. (a) Coupling diagram in in-line layout with one CT and one CQ. (b) I/O structure (side view) for dual-mode resonator. (c) Possible asymmetric response.

positive cross-coupling M_{46} and produces a TZ at the lower side the passband. Fig. 13(b) shows the typical response of the 6-2 passband filter. By simply changing the structures of the cross-couplings M_{13} and M_{46}, the two TZs can be realized at either side of the passband, thus facilitating the flexibility of design. The possible ideal asymmetric responses are shown in Fig. 13(c) and (d).

For further size reduction, the dual-mode resonator can be used as input/output (I/O) resonator. An L-shape coaxial probe can be inserted into the cavity from the top to form a capacitive feeding to the TEM mode of the dual-mode resonator, which is similar to that for a single TEM mode resonator. Taking a seven-pole bandpass filter as an example, the filter consists of one single-mode and three dual-mode resonators for one CT section and one CQ section. The original single-mode I/O resonator is replaced by a dual-mode one. The coupling diagram, the feeding structure, and a possible asymmetric response are shown in Fig. 14(a)–(c), respectively. Compared to the 6-2 configuration in Fig. 13, the configuration in Fig. 14 can realize a 7-3 in-line filter within the same volume.

IV. Three Design Examples

To demonstrate the applicability of the MDC dual-mode resonator, three 6-2 bandpass filters with in-line layout but different coupling topologies and responses in the 3.5-GHz band are designed and prototyped.

A. 6-2 Filter for Asymmetric Response With One CQ

A 6-2 in-line bandpass filter with an asymmetric response is designed and prototyped at center frequency $f_0 = 3.6$ GHz with a bandwidth BW $= 125$ MHz and a return loss level of 20 dB. The two TZs are at $\Omega = -1.3$ and 2.2 rad/s in the low-pass frequency domain. The coupling topology with the synthesized coupling coefficients is given in Fig. 15(a), in which the quadruplet 2-3-4-5 is realized by two dual-mode resonators, whereas resonators 1 and 6 are two single-mode conventional coaxial resonators.

The designed 6-2 filter is fabricated and tuned with the aid of the circuit model extraction technique presented in [20], [21], and [22]. The photograph of the prototyped filter hardware is shown in Fig. 15(b). The filter consists of two MDC dual-mode resonators and two single-mode coaxial resonators. The coupling between a single-mode resonator and the adjacent dual-mode resonator is realized by a partial height coupling window. The total inner dimension of the filter is $66 \times 15 \times 15$ mm^3. The size of the dual-mode resonator is

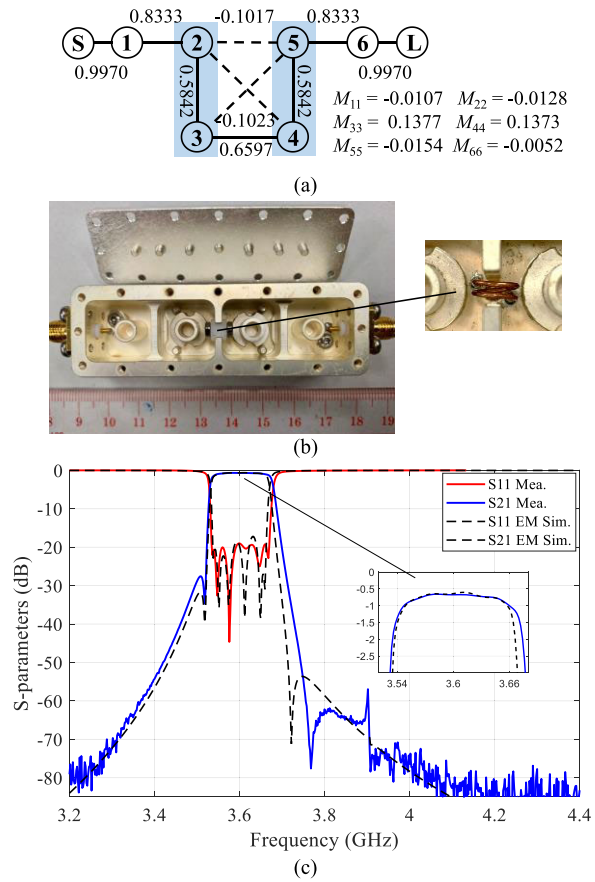

Fig. 15. (a) Target coupling diagram with synthesized coupling coefficients of the 6-2 in-line bandpass filter for asymmetric response with one CQ section. (b) Photograph of fabricated filter prototype (details of the coupling loop underneath dumbbell probe are zoomed in). (c) Measured and EM simulated responses of the prototyped filter.

the same as that of the single-mode cavity, and thus, a 33% volume saving is achieved.

The measured filter response is plotted in Fig. 15(c), superposed by the EM simulated response for comparison. The symmetry of TZs could be more satisfactory if the tunability of the grounded loop can be improved. Moreover, since the double turn grounded coupling loop in the CQ section is an asymmetric structure, a weak coupling between two HE_{11b} modes occurs, leading to a spike near 3.9 GHz at the level of -55 dB. The spurious mode can be further suppressed in a higher order filter with more single-mode resonators.

B. 6-2 Filter for Symmetric Response With Two CTs

For the second prototype filter, a 6-2 in-line bandpass filter with a symmetric response is designed and fabricated to demonstrate the claimed features of the CT section. The filter is designated at center frequency $f_0 = 3.6$ GHz with a bandwidth BW $= 200$ MHz and a return loss of 20 dB. Two TZs are designated at $\Omega = -2$ and 2 rad/s in the low-pass frequency domain to ensure the rejection level of -60 dB on both sides of the passband. The coupling topology with the synthesized coupling coefficients is given in Fig. 16(a), in which the triplet

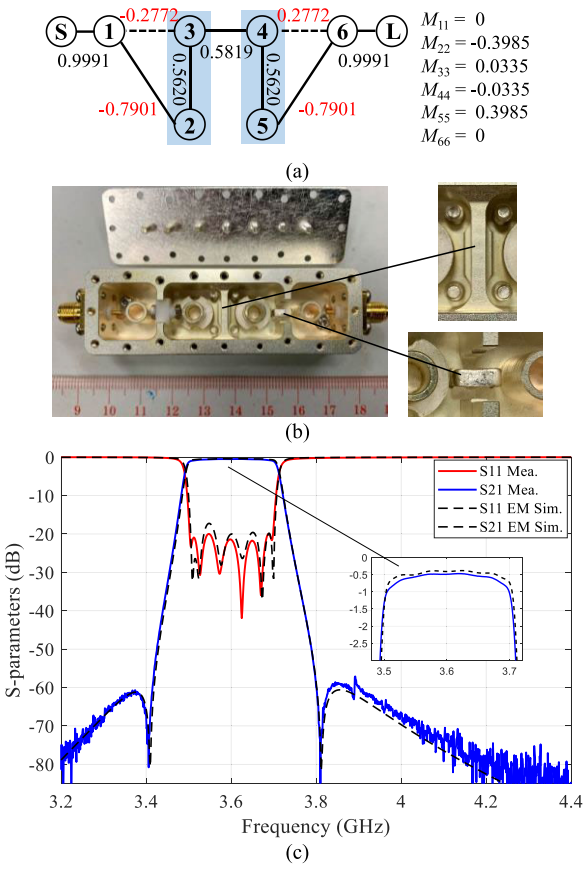

Fig. 16. (a) Target coupling diagram with synthesized coupling coefficients of the 6-2 in-line bandpass filter for symmetric response with two CT sections. (b) Photograph of fabricated filter prototype. (c) Measured and EM simulated responses of the prototyped filter.

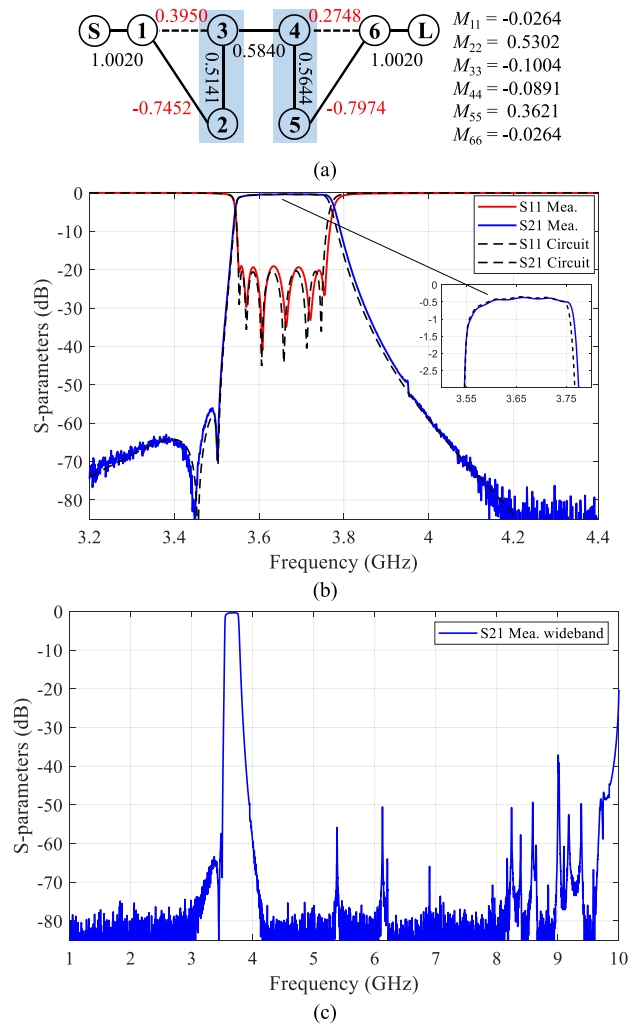

Fig. 17. (a) Target coupling diagram and synthesized coupling coefficients of the 6-2 in-line bandpass filter for asymmetric response with two CTs. (b) Narrowband measured and synthesized responses (with loss) of the prototyped filter. (c) Wideband response of the measured $|S_{21}|$.

sections 1-2-3 and 4-5-6 are both realized by one single-mode resonator and one MDC dual-mode resonator, respectively.

The designed 6-2 filter is prototyped and then tuned. The photograph of the prototyped filter hardware is shown in Fig. 16(b). The filter consists of two MDC dual-mode resonators and two single TEM mode resonators. The partial height coupling window is located between two dual-mode resonators to realize the mainline coupling M_{34} between two TEM modes. In this physical realization, the coupling between two dielectric HE_{11a} modes is very well isolated due to the use of the partial height coupling window. The grounded strip loops are used for M_{12} and M_{56}, the couplings between the single TEM mode and the dielectric HE_{11a} mode. Moreover, it can also be seen in Fig. 16(b) that two decoupling ridges are formed along both bottom edges of the partial height window to reduce the couplings M_{23} and M_{45} among the dual modes in each of the MDC dual-mode resonators.

The measured filter response is presented in Fig. 16(c), superposed by the EM simulated response for comparison, showing that the prototyped filter achieves a return loss of more than 20 dB with a nearly equal ripple response within the prescribed passband. The measured insertion loss at f_0 is 0.49 dB, which is slightly higher than that of the EM simulated response. The TZs of measured response are located at 3.406 and 3.810 GHz, which matches the designated positions very well. As far as the spurious resonance is concerned, since the grounded coupling loop is simple and symmetric, the pushed away HE_{11b} mode is maximally suppressed. In addition, the two preserved tuning screws in each dual-mode resonator can also help further compensate the aggregate asymmetry of the total structure to further suppress the resonance of the HE_{11b} mode. As a result, the spurious resonance of the prototype filter occurring at 3.9 GHz is at the level of around -60 dB.

C. 6-2 Filter for Asymmetric Response With Two CTs

For the third prototype filter, a 6-2 in-line bandpass filter with an asymmetric response is designed and prototyped. Similar to the second prototype filter, the filter consists of two CT sections, and both sections realize a TZ at the lower side of the passband. The filter is designated at center frequency $f_0 = 3.65$ GHz with a bandwidth BW $= 200$ MHz and a return loss of 20 dB. The two TZs are at $\Omega = -1.5$ and -2 rad/s in the low-pass frequency domain to ensure a sharp rejection curve at the lower side of the passband. The coupling diagram and the synthesized coupling coefficients are given in Fig. 17(a). The

TABLE I
EXTRACTED UNLOADED Q FACTORS FOR EACH RESONATOR OF THE 6-2 IN-LINE BANDPASS FILTER PROTOTYPE

	Q_1	Q_2	Q_3	Q_4	Q_5	Q_6
Circuit	1600	1550	1900	1900	1550	1600
Extracted	932	1504	2054	1703	1540	1518

first triplet 1-2-3 and the second triplet section 4-5-6 are responsible for the TZs at -1.5 and -2 rad/s, respectively, which can be realized by partial width inductive windows.

The designed 6-2 filter with an asymmetric response is fabricated and fine-tuned. The measured filter response is plotted in Fig. 17(b) and is superposed with the response of the circuit model with uneven unloaded Qs according to the previous eigenmode analysis. The estimated unloaded Qs for each resonator are listed in Table I. The extracted unloaded Qs from the measured data are also listed in Table I for comparison. It can be found that the unloaded Q of the input resonator Q_1 is unexpectedly lower than that of the ideal circuit model due to the rough soldering of the input probing structure, which deteriorates the insertion loss. The measured insertion loss at f_0 is 0.4 dB, which is comparable to that of the circuit model. The two measured TZs are located at 3.449 and 3.502 GHz, which meets the prescribed positions very well. The spurious resonance of the HE_{11b} mode is not apparent at the higher rejection band in this case.

Fig. 17(c) shows the wideband response from 1 to 10 GHz of the prototyped filter. It can be observed that a wide spurious-free frequency band (below -50 dB) can be obtained up to 9 GHz ($2.5 \times f_0$), demonstrating the superiority of a dual-mode resonator with two dissimilar fundamental modes in terms of spurious performance.

V. CONCLUSION

In this article, a novel dual-mode resonator structure utilizing two dissimilar fundamental modes, namely, MDC dual-mode resonator, is proposed and put into various practical uses. The dual-mode resonator occupies the same volume and exhibits similar unloaded Q as those of a conventional metal coaxial resonator. The basic working principle of the resonator is revealed, and electric properties are analyzed with the EM simulation. Various coupling schemes adopting the proposed dual-mode resonator are also discussed in detail. The MDC dual-mode resonator provides a very practical option to realize a high-order filter in the in-line layout. Two cross-coupling sections, namely, the quadruplet section that consists of two MDC dual-mode resonators and the triplet section that comprises one single-mode resonator and one MDC dual-mode resonator, are investigated intensively. To demonstrate the claimed features, a 6-2 in-line filter with a CQ section and two 6-2 in-line filters, each has two CT sections, are designed and prototyped, showing great flexibility in realizing both symmetric and asymmetric responses. The experimental results show that the MDC dual-mode resonator is friendly in layout, easy to fabricate, and fully compatible with the conventional single-mode coaxial resonator. It is expected that the new dual-mode resonator will provide the wireless industry with a promising option in designing bandpass filters with a compact size, in-line layout, and wide spurious rejection band for future wireless communication systems.

REFERENCES

[1] D. Liang, X. Zhang, B. Yang, and D. Young, "Overview of base station requirements for RF and microwave filters," in *IEEE MTT-S Int. Microw. Symp. Dig.*, Nov. 2021, pp. 46–49.

[2] W. H. Harrison, "A miniature high-Q bandpass filter employing dielectric resonators," *IEEE Trans. Microw. Theory Techn.*, vol. MTT-16, no. 4, pp. 210–218, Apr. 1968.

[3] S. B. Cohn, "Microwave bandpass filters containing high-Q dielectric resonators," *IEEE Trans. Microw. Theory Techn.*, vol. MTT-16, no. 4, pp. 218–227, Apr. 1968.

[4] J. K. Plourde and C.-L. Ren, "Application of dielectric resonators in microwave components," *IEEE Trans. Microw. Theory Techn.*, vol. MTT-29, no. 8, pp. 754–770, Aug. 1981.

[5] S. J. Fiedziuszko, "Dual-mode dielectric resonator loaded cavity filters," *IEEE Trans. Microw. Theory Techn.*, vol. MTT-30, no. 9, pp. 1311–1316, Sep. 1982.

[6] C. Wang, K. A. Zaki, and A. E. Atia, "Dual mode combined dielectric and conductor loaded cavity filters," in *IEEE MTT-S Int. Microw. Symp. Dig.*, Jun. 1997, pp. 1103–1106.

[7] L. Accatino, G. Bertin, M. Mongiardo, and G. Resnati, "Dual-mode filters with grooved/splitted dielectric resonators for cellular-radio base stations," *IEEE Trans. Microw. Theory Techn.*, vol. 50, no. 12, pp. 2882–2889, Dec. 2002.

[8] H. Hu and K.-L. Wu, "A TM_{11} dual-mode dielectric resonator filter with planar coupling Configuration," *IEEE Trans. Microw. Theory Techn.*, vol. 61, no. 1, pp. 131–138, Jan. 2013.

[9] I. C. Hunter, J. D. Rhodes, and V. Dassonville, "Dual-mode filters with conductor-loaded dielectric resonators," *IEEE Trans. Microw. Theory Techn.*, vol. 47, no. 12, pp. 2304–2311, Dec. 1999.

[10] R. J. Cameron, C. M. Kudsia, and R. R. Mansour, *Microwave Filters for Communication Systems*. 2nd ed. Hoboken, NJ, USA: Wiley, 2018.

[11] V. Walker and I. C. Hunter, "Design of triple mode $TE_{01\delta}$ resonator transmission filters," *IEEE Microw. Wireless Compon. Lett.*, vol. 12, no. 6, pp. 215–217, Jun. 2002.

[12] S.-W. Wong, Z.-C. Zhang, S.-F. Feng, F.-C. Chen, L. Zhu, and Q.-X. Chu, "Triple-mode dielectric resonator diplexer for base-station applications," *IEEE Trans. Microw. Theory Techn.*, vol. 63, no. 12, pp. 3947–3953, Dec. 2015.

[13] M. S. Bakr, I. C. Hunter, and W. Bösch, "Miniature triple-mode dielectric resonator filters," *IEEE Trans. Microw. Theory Techn.*, vol. 66, no. 12, pp. 5625–5631, Dec. 2018.

[14] C. Tomassoni, S. Bastioli, and R. V. Snyder, "Compact mixed-mode filter based on TE_{101} cavity mode and $TE_{01\delta}$ dielectric mode," *IEEE Trans. Microw. Theory Techn.*, vol. 64, no. 12, pp. 4434–4443, Dec. 2016.

[15] Á. A. San-Blas, M. Guglielmi, J. C. Melgarejo, Á. Coves, and V. E. Boria, "Design procedure for bandpass filters based on integrated coaxial and rectangular waveguide resonators," *IEEE Trans. Microw. Theory Techn.*, vol. 68, no. 10, pp. 4390–4404, Oct. 2020.

[16] Y. Chen, Y. Zhang, and K.-L. Wu, "A dual-mode monoblock dielectric bandpass filter using dissimilar fundamental modes," *IEEE Trans. Microw. Theory Techn.*, vol. 69, no. 8, pp. 3811–3819, Aug. 2021.

[17] S. Tamiazzo, G. Macchiarella, and F. Seyfert, "Path filters: A class of true inline topologies with transmission zeros," *IEEE Trans. Microw. Theory Techn.*, vol. 70, no. 1, pp. 850–863, Jan. 2022.

[18] Y. Chen and K.-L. Wu, "Metal-dielectric coaxial dual-mode resonator for compact inline bandpass filters," in *IEEE MTT-S Int. Microw. Symp. Dig.*, Jun. 2023, pp. 403–405.

[19] X. Yin, "Accurate extraction of coupling matrix for coupled resonator filters," in *IEEE MTT-S Int. Microw. Symp. Dig.*, Jun. 2012, pp. 1–3.

[20] M. Meng and K.-L. Wu, "An analytical approach to computer-aided diagnosis and tuning of lossy microwave coupled resonator filters," *IEEE Trans. Microw. Theory Techn.*, vol. 57, no. 12, pp. 3188–3195, Dec. 2009.

[21] H. Hu and K.-L. Wu, "A generalized coupling matrix extraction technique for bandpass filters with uneven-qs," *IEEE Trans. Microw. Theory Techn.*, vol. 62, no. 2, pp. 244–251, Feb. 2014.

[22] P. Zhao and K.-L. Wu, "Model-based vector-fitting method for circuit model extraction of coupled-resonator diplexers," *IEEE Trans. Microw. Theory Techn.*, vol. 64, no. 6, pp. 1787–1797, Jun. 2016.

Yuliang Chen (Graduate Student Member, IEEE) received the B.Eng. degree in electromagnetic field and wireless technology from Northwestern Polytechnical University, Xi'an, China, in 2017. He is currently pursuing the Ph.D. degree at the Department of Electronic Engineering, The Chinese University of Hong Kong, Hong Kong SAR.

His current research interests include miniaturization techniques and robot automatic tuning of microwave filters for wireless communications.

Mr. Chen was a recipient of the Best Paper Award of the 2020 IEEE (HK) AP/MTT Postgraduate Conference.

Ke-Li Wu (Fellow, IEEE) received the B.S. and M.Eng. degrees from the Nanjing University of Science and Technology, Nanjing, China, in 1982 and 1985, respectively, and the Ph.D. degree from Laval University, Québec, QC, Canada, in 1989.

From 1989 to 1993, he was a Research Engineer with McMaster University, Hamilton, ON, Canada. He joined COM DEV (now Honeywell Aerospace), Cambridge, ON, Canada, in 1993, where he was a Principal Member of Technical Staff. Since 1999, he has been with The Chinese University of Hong Kong, Hong Kong, where he is currently a Professor and the Director of the Radiofrequency Radiation Research Laboratory. His current research interests include electromagnetic (EM)-based circuit domain modeling of high-speed interconnections, robot automatic tuning of microwave filters, decoupling techniques of multi-input–multioutput (MIMO) antennas, and IoT technologies.

Prof. Wu is a member of the IEEE MTT-5 Technical Committee. He was a recipient of the 1998 COM DEV Achievement Award and the Asia-Pacific Microwave Conference Prize twice in 2008 and 2012, respectively. He was an Associate Editor of the IEEE TRANSACTIONS ON MICROWAVE THEORY AND TECHNIQUES from 2006 to 2009.